

# 1 $\mu$ bialSim: constraint-based dynamic 2 simulation of complex microbiomes

3 Denny Popp<sup>1</sup> and Florian Centler<sup>1\*</sup>

4

5 <sup>1</sup> Department of Environmental Microbiology, UFZ – Helmholtz Centre for Environmental Research,  
6 Leipzig, Germany

7

8 \* Corresponding author

9 E-mail: [florian.centler@ufz.de](mailto:florian.centler@ufz.de)

## 10 **Abstract**

11 Microbial communities are pervasive in the natural environment, associated with many animal hosts,  
12 and of increasing importance in biotechnological applications. The complexity of these microbial  
13 systems makes the underlying mechanisms driving their dynamics difficult to identify. While  
14 experimental meta-OMICS techniques are routinely applied to record the inventory and activity of  
15 microbiomes over time, it remains difficult to obtain quantitative predictions based on such data.  
16 Mechanistic, quantitative mathematical modeling approaches hold the promise to both provide  
17 predictive power and shed light on cause-effect relationships driving these dynamic systems.  
18 We introduce  $\mu$ bialSim (pronounced “microbialsim”), a dynamic Flux-Balance-Analysis-based (dFBA)  
19 numerical simulator which is able to predict the time course in terms of composition and activity of  
20 microbiomes containing 100s of species in batch or chemostat mode. Activity of individual species is  
21 simulated by using separate FBA models which have access to a common pool of compounds,  
22 allowing for metabolite exchange. A novel augmented forward Euler method ensures numerically

23 accuracy by temporarily reducing the time step size when compound concentrations decrease  
24 rapidly due to high compound affinities and/or the presence of many consuming species. We present  
25 three exemplary applications of  $\mu$ bialSim: a batch culture of a hydrogenotrophic archaeon, a  
26 syntrophic methanogenic biculture, and a 773-species human gut microbiome which exhibits a  
27 complex and dynamic pattern of metabolite exchange.  
28 Focussing on metabolite exchange as the main interaction type,  $\mu$ bialSim allows for the mechanistic  
29 simulation of microbiomes at their natural complexity. Simulated trajectories can be used to  
30 contextualize experimental meta-OMICS data, and hypotheses on cause-effect relationships driving  
31 community dynamics can be derived based on scenario simulations.  
32  $\mu$ bialSim is implemented in Matlab and relies on the COBRA Toolbox or CellNetAnalyzer for FBA  
33 calculations. The source code is available under the GNU General Public License v3.0 at  
34 <https://git.ufz.de/UMBSysBio/microbialsim>.

## 35 Introduction

36 Microbial communities are ubiquitous in nature, thriving in diverse habitats ranging from the deep  
37 subsurface [1] over digestive tracts of higher animals [2] to the upper troposphere [3]. They are self-  
38 organizing entities which both modulate the environment they are embedded in, as well as their own  
39 constituents in terms of abundance of individual member populations. Typical natural and  
40 engineered microbiomes engage in numerous metabolic and non-metabolic interactions and contain  
41 a large fraction of not-yet cultured species. The resulting complexity makes microbiomes notoriously  
42 difficult to study. Meta-OMICS techniques help to uncover the metabolic potential and current  
43 activity of microbiomes. However, most analyses based on such data remains observational in nature  
44 and cannot be used to derive quantitative predictions. The mathematical modeling of microbiomes  
45 holds the promise to move from observation to a more quantitative understanding of microbiome  
46 dynamics and underlying mechanisms [4–7].

47 Focusing on metabolic interaction, a number of dynamic community modeling approaches have been  
48 proposed in which activity of individual species is modeled using constraint-based techniques based  
49 on genome-scale metabolic network reconstructions [8]. Some of these approaches require the  
50 definition of a secondary community objective in addition to the standard growth maximization  
51 objective for individual species (e.g., d-OptCom, [9]), a priority list of objectives (DFBALab [10]), or a  
52 pre-allocation of compounds to competing species [11]. Other models additionally allow for  
53 parameter calibration (MCM [12]), or for the inclusion of space either simulating populations  
54 (COMETS [13], MetaFlux [14]) or individual microbial cells following a rule-based approach  
55 (BacArena, [15]). With the exception of the last approach, typically only microbiomes of few species  
56 have been considered in simulations yet. In order to be able to mirror the diversity of natural  
57 microbiomes, we developed  $\mu$ bialSim. Our simulator is based on the dynamic Flux-Balance-Analysis  
58 approach and does not require the definition of any additional objectives or the pre-allocation of  
59 compounds. It allows for the simulation of well-mixed microbiomes of high diversity under batch and  
60 chemostat conditions with high numerical accuracy due to a novel numerical integration scheme.

## 61 **Design and Implementation**

### 62 **Overview**

63 In order to simulate the fate and metabolic activity of a microbial community we follow the  
64 compartmentalized approach in which activity and growth of individual species is modeled by  
65 separate genome-scale metabolic network models following the Flux-Balance-Analysis approach  
66 (FBA, [16]). All species have access to a common set of pool compounds. This allows for competition  
67 between species as they try to consume the same pool compound and cross-feeding if one species  
68 produces a pool compound another is able to use for growth. Instead of restricting analysis to steady  
69 state dynamics for which the community composition must be defined as a model input (e.g.,  
70 [17,18]), we follow the dynamic FBA approach [19] in order to be able to simulate dynamic shifts in  
71 microbiomes as a consequence of the system's dynamics. In this approach, the steady-state

72 assumption underlying FBA is assumed to hold true for the duration of the numerical integration  
73 step. FBA-computed growth and compound exchange rates are then used to update the state  
74 variables of the model which encompass microbial biomass and pool compound concentrations.  
75  $\mu$ bialSim is implemented as Matlab code and relies on either the COBRA Toolbox [20] or  
76 CellNetAnalyzer [21] for performing FBA computations. This allows for the easy incorporation of FBA  
77 models prepared with either softwares in a community model. Space is neglected in the model,  
78 hence assuming a well-mixed environment similar to a well-stirred bioreactor. Both batch and  
79 chemostat operation can be simulated. Both compounds and microbial populations can be defined to  
80 be part of the bioreactor inflow.

## 81 Mathematical description

82 The system state is given by  $(C, X)$ , with  $C = (C_1, \dots, C_m)$  referring to the concentrations (in mM) of  $m$   
83 pool compounds present in the bioreactor and  $X = (X_1, \dots, X_n)$  referring to the abundance (in gDW/L) of  
84  $n$  microbial populations. For each of these populations, the exchange reactions in their metabolic  
85 network model which describe the transport of a metabolite across the cell membrane need to be  
86 identified. Not all of these reactions need to be coupled to pool compounds. For example  
87 metabolites assumed not to be growth-limiting can be ignored. With  $k$  the number of coupled  
88 exchange reactions for species  $j$ ,  $coupReact^j = (r_1, \dots, r_k)$  records the reaction IDs of the respective  
89 exchange reactions,  $coupComp^j = (idx_i, \dots, idx_k)$  the indices of the corresponding compounds in  $C$ ,  
90  $coupSense^j = (s_i, \dots, s_k)$  the directionality of the exchange reaction with the reaction proceeding in the  
91 forward direction indicating metabolite excretion for  $s = 1$  and metabolite uptake for  $s = -1$ ,  
92  $coupVmax^j$  the maximal uptake fluxes, and  $coupKs^j$  the corresponding Monod constants (see below).  
93 The dynamics of the system is then given by two sets of ordinary differential equations. Microbial  
94 dynamics for species  $j$  is given by

$$\frac{dX_j}{dt} = (X_j^{inflow} - X_j) \frac{q}{V} + \mu_j X_j \quad (\text{Equation 1})$$

95 with microbial concentration in the inflow  $X_i^{inflow}$  (gDW/L), flow rate  $q$  (L/h), bioreactor volume  $V$  (L),  
 96 and specific growth rate  $\mu_i$  (1/h). The dynamics of pool compound  $i$  in the bioreactor is given by

$$\frac{dC_i}{dt} = (C_i^{inflow} - C_i) \frac{q}{V} + \sum_{\substack{j=1, i \in \text{coupComp}^j \\ \text{with } i \text{ the } k\text{-th element}}}^n \text{coupSense}_k^j \times v_{\text{coupReac}_k^j} \times X_j \quad (\text{Equation 2})$$

97 with inflow concentration  $C_i^{inflow}$  (mM) and flux of the exchange reaction  $v_j^i$  (mmol/gDW/h) which is  
 98 the  $i$ -th reaction of the  $j$ -th species.

99 The specific growth rates  $\mu$  and exchange fluxes  $v$  are derived by solving individual FBA problems for  
 100 all species individually. For this purpose, current compound concentrations in the bioreactor need to  
 101 be translated to maximal allowable uptake rates. This is commonly done by assuming Monod-type  
 102 kinetics. For the  $i$ -th exchange reaction of species  $j$  which is coupled to pool compound  $\text{coupComp}_i^j$ ,  
 103 the current maximal uptake rate is given by

$$v_{\text{maxUptake}, i}^j = \text{coupVmax}_i^j \frac{C_{\text{coupComp}_i^j}}{\text{coupKs}_i^j + C_{\text{coupComp}_i^j}}. \quad (\text{Equation 3})$$

## 104 Numerical integration scheme

105 While  $\mu\text{bialSim}$  can make use of Matlab solvers for numerically integrating Equations 1-2 (options  
 106 `solverPars.solverType` and `solverPars.solver`), the computational costs quickly  
 107 becomes prohibitive for more complex microbial communities. Instead, we have implemented a  
 108 novel augmented forward Euler method in  $\mu\text{bialSim}$ . The forward Euler method uses the system state  
 109 at time  $t$ , evaluates Equations 1-2 and uses computed rates to derive the system state at time  $t + \Delta t$ ,  
 110 with  $\Delta t$  being the integration step size:

$$X(t + \Delta t) = X(t) + \Delta t \times \frac{dX(t)}{dt}, \quad (\text{Equation 4})$$

$$C(t + \Delta t) = C(t) + \Delta t \times \frac{dC(t)}{dt}.$$

111 For syntrophic interactions such as in syntrophic propionate degradation (see Example 2), a  
112 compound produced by one species (here: hydrogen), needs to be quickly consumed by the  
113 syntrophic partner (here: a methanogenic archaeon) as propionate degradation is  
114 thermodynamically only feasible for low hydrogen concentrations. This means that typically, the  
115 partner features an effective uptake of the compound with a small  $K_s$  value in Equation 3. As  
116 consumption can become much faster than production, a very negative rate for hydrogen may result  
117 in Equation 2. This can lead to the computation of negative concentrations during an integration step  
118 (Equation 4). Similarly, this can also be caused by many species competing for a highly attractive  
119 compound. Simply setting negative values to zero in each integration step induces a numerical error.  
120 Instead, choosing a smaller integration step size can solve this problem, but might significantly  
121 prolong simulation time. Hence, in  $\mu$ bialSim the integration step size is reduced only temporarily  
122 whenever this situation occurs in order to avoid numerical error at an affordable increase in  
123 computational cost. The time step size is reduced in such a way that the concentration of compound  
124  $o$  at the next time step is close to its steady-state concentration under the assumption that the  
125 production process remains constant. We first identify all species which are either producing or  
126 consuming compound  $o$ . We then compute the current total production rate  $p$  and the current total  
127 uptake rate  $u$  for the compound by summing across the identified species. Additionally, let  $f$  describe  
128 the current rate of concentration change for compound  $o$  due to a prescribed flow if a chemostat is  
129 simulated. The steady-state condition is then given by  $p = u - f$ . Treating  $p$  as fixed, we find that the  
130 right-hand side of this equation depends on the compound concentration  $C_o$  when combining  
131 Equations 2 and 3:

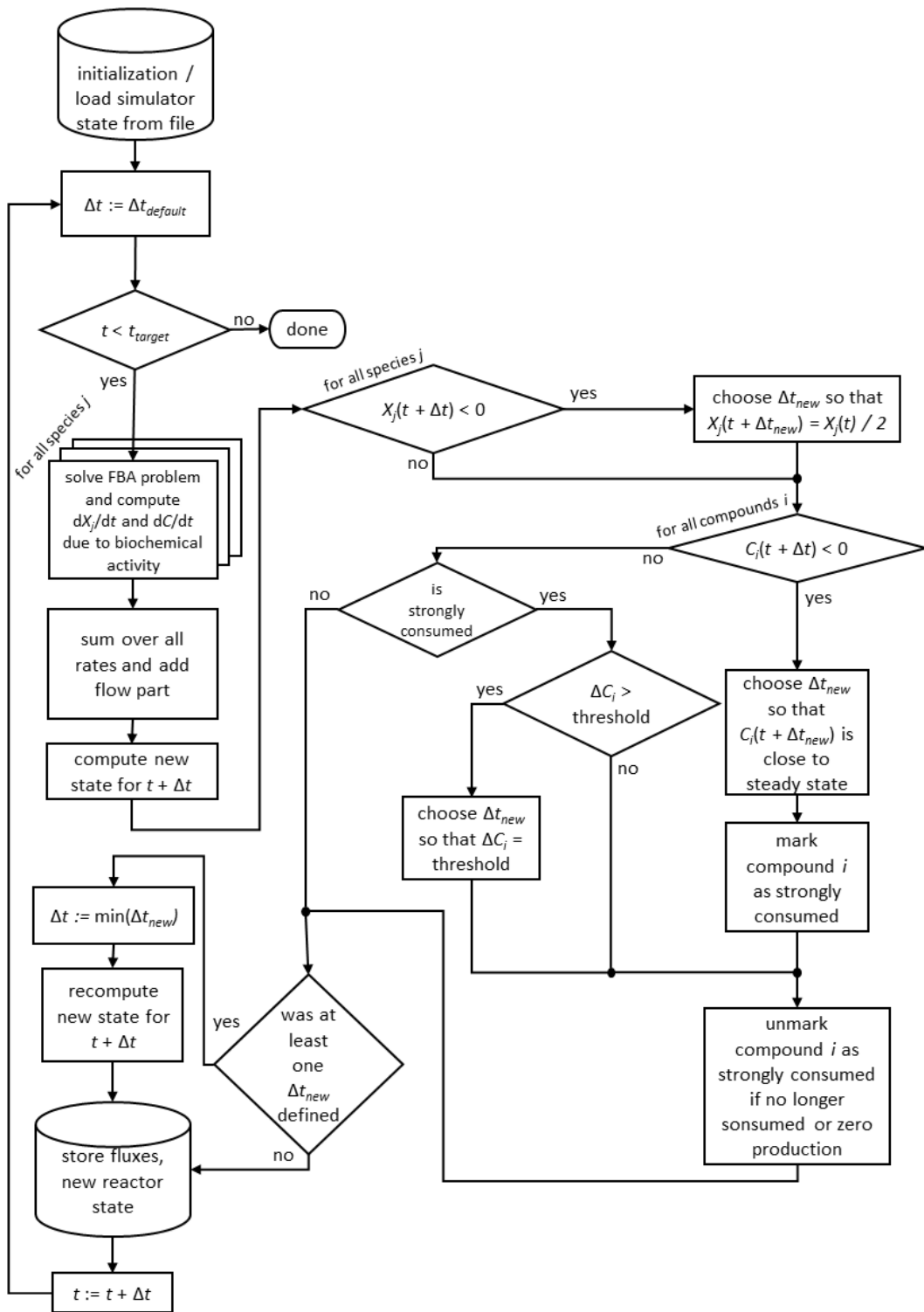
$$u - f = \sum_{j \text{ is a consuming species}} |Vmax^j| \frac{C_o}{K_s^j + C_o} \times X_j - (C_o^{inflow} - C_o) \frac{q}{V}. \quad (\text{Equation 5})$$

132 Under the assumption that compound  $o$  is the growth-limiting factor for the second species (i.e., the  
133 maximal uptake rate is indeed realized) and that growth remains viable for smaller concentrations,  
134 the steady-state concentration  $C_o^*$  for compound  $o$  can be found by reducing concentration  $C_o$  in

135 Equation 5 until  $p = u(C_o^*) - f(C_o^*)$ . The time step size  $\Delta t$  which leads  $C_o(t + \Delta t)$  to be evaluated to  $C_o^*$   
136 can then be computed with the help of Equation 4 to:

$$\Delta t = (C_o^* - C_o(t)) / \frac{dC_o(t)}{dt}. \quad (\text{Equation 6})$$

137 If for more than one chemical compound negative concentrations were calculated using the default  
138 time step size, for each of these compounds the described scheme is applied and ultimately the  
139 smallest time step size used. We note that reducing the time step size does not require the  
140 recomputation as FBA problems, as only  $\Delta t$  changes in Equation 4. For the next time step, the default  
141 time step size is restored. Compounds which required the reduction of the time step size are flagged  
142 as strongly consumed compounds, as their consumption rate surpassed their production rate. In  
143 order to avoid oscillatory behavior for these compounds,  $\mu\text{bialSim}$  allows to additionally restrict the  
144 time step size in subsequent iteration steps such that the concentration change of these compounds  
145 does not surpass a given threshold (parameter `solverPars.maxDeviation`). If negative  
146 biomass concentrations occur, the time step size is reduced such that the biomass concentration is at  
147 most reduced by a factor of two. The flowchart in Fig 1 depicts the complete algorithmic logic of the  
148 augmented forward Euler method implemented in  $\mu\text{bialSim}$ .



149

150 **Fig 1. The augmented forward Euler scheme implemented in  $\mu$ bialSim.** In each numerical  
 151 integration step, first the FBA solutions are computed for all member species of the simulated  
 152 microbiome. The new system state is then computed using obtained rates and the default time step  
 153 size. If negative concentration values for biomasses or compounds occur, the time step size is  
 154 reduced as required.



## 155 Features

156 FBA computations can have non-unique solutions such that different flux distributions lead to the  
157 same maximal growth rate. In dFBA simulations, this can cause discontinuities in intracellular fluxes  
158 over time. To avoid this, `μbialSim` implements two features which can individually or in tandem be  
159 activated. The first feature is a secondary optimization step which seeks to realize the optimal  
160 growth rate as determined by the initial FBA computation, but with minimal fluxes, known as  
161 parsimonious FBA [22]. The second feature tries to realize the optimal growth rate by a flux  
162 distribution that most resembles the flux distribution which was active in the last integration step, a  
163 methodology similar to the minimization of metabolic adjustment approach (MOMA, [23]) which has  
164 been applied in the context of dFBA before [24]. Simulation results can be stored at each integration  
165 step in individual files or in a single result file at the end of the simulation. The former feature  
166 (parameter `solverPars.recording`) is helpful for complex simulations as simulated data is not  
167 lost in case of unforeseen server downtimes or other computational calamities. A subsequent  
168 simulator run can use the saved data to initialize the simulator and continue the interrupted  
169 simulation run (parameter `solverPars.readInitialStateFrom`).

170 As loading SBML files and preparing the corresponding data structures can take a while for complex  
171 microbiomes, the data structures of the loaded models can be saved as a single file and be used in  
172 subsequent simulation runs to speed up initialization (parameter  
173 `solverPars.saveLoadedModelToFile`).

174 Once the simulation is done, `μbialSim` computes the overall activity during the simulation for all  
175 exchange fluxes of all species (including both exchange reactions which were coupled to pool  
176 compounds and those which were not) if desired (parameter `solverPars.doMassBalance`).  
177 This indicates the total compound turnover per species in terms of compound production minus  
178 consumption (in mM), and the resulting increase in biomass concentration (in gDW/L). Additionally,  
179 three figures to visualize the simulation result are automatically generated. The first figure gives a  
180 quick overview over the temporal evolution of all microbial biomass concentrations and all pool

181 compound concentrations over time. In the second figure, all biomass concentrations are plotted in  
182 one panel as an offset to the initial biomass concentration, to make dynamics easy to inspect for  
183 species having very different initial biomass concentrations, and individual panels for each pool  
184 compound. The third figure contains two panels for each microbial species and shows the evolution  
185 of coupled exchange reactions, and exchange reactions which were not coupled. Only non-zero  
186 exchange fluxes are shown.

## 187 Setting up and running a microbiome simulation

188 The bioreactor and its operational parameters are defined in the function  
189 `reactorDefinition_*.m`. Here, the reactor volume, flow rate, and the list of pool compounds  
190 is defined. Additionally, initial concentrations for compounds and biomasses are specified, as well as  
191 their concentration in the inflow in case a chemostat is to be simulated.  
192 Loading a FBA model of an individual species of the microbiome to be simulated is recommended to  
193 be done in two steps. First, the model is loaded by using the appropriate commands of either the  
194 COBRA Toolbox or CellNetAnalyzer in the Matlab function `prepareFBAmodel_*.m`. After loading,  
195 if necessary, general constraints on particular reactions can be set, for example to implement a  
196 particular scenario. Next, the reaction IDs of the biomass reaction and the non-growth associated  
197 maintenance reaction (NGAM) need to be specified. Reaction IDs refer to their running order in the  
198 SBML file (or corresponding CellNetAnalyzer data structure). Furthermore, all exchange reactions  
199 need to be identified by their IDs and their directionality, that means whether a positive  
200 flux indicates compound secretion ( $Sense = 1$ ) or compound uptake ( $Sense = -1$ ). Finally the  
201 subset of exchange reactions are identified, which will be coupled to pool compounds present in the  
202 bioreactor in the vector `IDs`. The mapping of coupled reactions to reactor compounds is done in the  
203 vector `reactorCompoundIDs` of length  $k$ , with  $k$  indicating the number of coupled reactions. The  
204 entry at the  $i$ -th position specifies for the  $i$ -th coupled reaction, as defined before in the vector `IDs`,  
205 the index of the reactor compound (referring to vector `reactor.compounds`) to which the

206 exchange reaction is coupled. After this general setup of the FBA model, model parameters are  
207 defined in the second step in the function `parametrizeFBAmodel_*.m`. Here, the values for  
208 NGAM, and  $v_{max}$  and  $K_S$  to define uptake kinetics for all coupled compounds are set.  
209 Finally, the target simulation time, default time step size and other options (see Features) and  
210 numerical accuracy parameters are set in the main simulator file `microbialSimMain.m`.

## 211 Results

212 We present three exemplary applications of `μbialSim` simulating batch growth of a monoclonal  
213 hydrogenotrophic culture, a syntrophic biculture transforming propionate to methane, and a 773  
214 species human gut microbiome. In all examples, a bioreactor volume of 1 L and a default time step  
215 size of  $\Delta t_{default} = 0.002$  h was chosen. The simulation end time was set to  $t_{target} = 1$  h for the mono- and  
216 binary culture, and to 0.3 h for the human microbiome example. All simulations were run in Matlab  
217 R2018a on an Intel® Xeon® CPU E5-4620 v2@2.6GHz with 32 cores. Up to 64GB of RAM were  
218 required to simulate the 773 species microbiome.

### 219 Batch culture of *Methanococcus maripaludis*

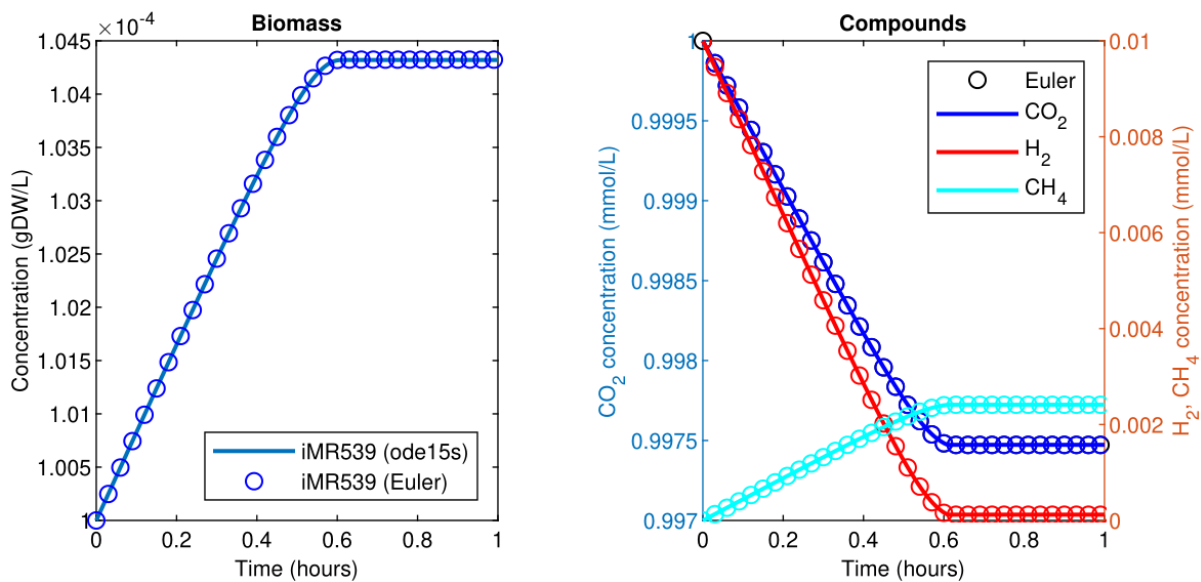
220 A batch culture of the hydrogenotrophic methanogen *M. maripaludis* was simulated using an  
221 established genome-scale FBA model [25]. The archaeon transforms  $H_2$  and  $CO_2$  to  $CH_4$ . Excess  $CO_2$   
222 was provided such that  $H_2$  was the growth limiting factor. Model parameters and initial conditions  
223 are listed in Table 1. Simulation results show an almost linear growth of *M. maripaludis* until  $t = 0.6$  h  
224 when  $H_2$  becomes depleted and growth stops (Fig 2). Simulations using Matlab's ODE solver `ode15s`  
225 and the novel augmented forward Euler method lead to identical results (Fig 2) with comparable  
226 simulation times (2.2 minutes for Matlab's solver and 3.4 minutes for the Euler method).

227

228 **Table 1. Model parameters and initial conditions for Example 1.**

Model parameters for <i>M. maripaludis</i> model iMR539				Initial conditions		
$\mu$ (1/d)	$v_{max}^a$ (mmol/ gDW/h)	$K_s$ (mM)	NGAM (mmol ATP/gDW/h)	Biomass (gDW/L)	H <sub>2</sub> (mM)	CO <sub>2</sub> (mM)
2.1 [26]	189.3	$4.375 \times 10^{-4}$ [26]	5.1176 [25]	$1.0 \times 10^{-4}$	0.01	1.0

229 <sup>a</sup>Was chosen such that the maximal FBA-predicted growth rate matched the specific growth rate  $\mu$   
 230 reported in first table column.



231  
 232 **Fig 2. Simulating a hydrogenotrophic batch culture.** A *M. maripaludis* population converts H<sub>2</sub> and  
 233 CO<sub>2</sub> to CH<sub>4</sub> until H<sub>2</sub> becomes depleted. Both Matlab's ode15s ODE solver (lines) and  $\mu$ bialSim's novel  
 234 augmented forward Euler method (symbols, every 15th data point is plotted) lead to identical  
 235 results.

236 Co-culture of *Syntrophobacter fumaroxidans* and *Methanospirillum*

237 *hungatei*

238 The syntrophic conversion of propionate to methane was simulated by using a binary FBA model  
239 community of *S. fumaroxidans* and *M. hungatei* which has previously been simulated at steady state  
240 [18]. Model parameters are listed in Table 2, choosing an initial relative biomass ratio of 3:4 (*M.*  
241 *hungatei*:*S. fumaroxidans*) as previously [18]. Initial compound concentrations were set to 20 mM for  
242 propionate, 0.9561  $\mu\text{M}$  for  $\text{H}_2$  and 8.215  $\mu\text{M}$  for  $\text{CO}_2$  which was considered not to be growth limiting  
243 for the methanogen. Being produced by *S. fumaroxidans* and quickly consumed by *M. hungatei*,  $\text{H}_2$   
244 was flagged as a strongly consumed compound in the simulation. The time step size became reduced  
245 and reached a minimum just prior to the depletion of  $\text{H}_2$  as growth of *S. fumaroxidans* ceased due to  
246 low propionate concentrations at  $t = 0.76$  h (Fig 3). Except for  $\text{H}_2$ , simulation results agreed well if  
247 using Matlab's ODE solver or the novel numerical Euler scheme. For  $\text{H}_2$ , minor fluctuations around  
248 the ODE result were apparent when using the Euler scheme (Fig 3). Most notably, the final  $\text{H}_2$   
249 concentration was 0 instead of the ODE predicted (small) concentration of 43.9 pM. Simulation times  
250 remained below 30 minutes for both Matlab's ODE solver (9.7 minutes) and the augmented forward  
251 Euler method (22.6 minutes).

252

253

254

255

256

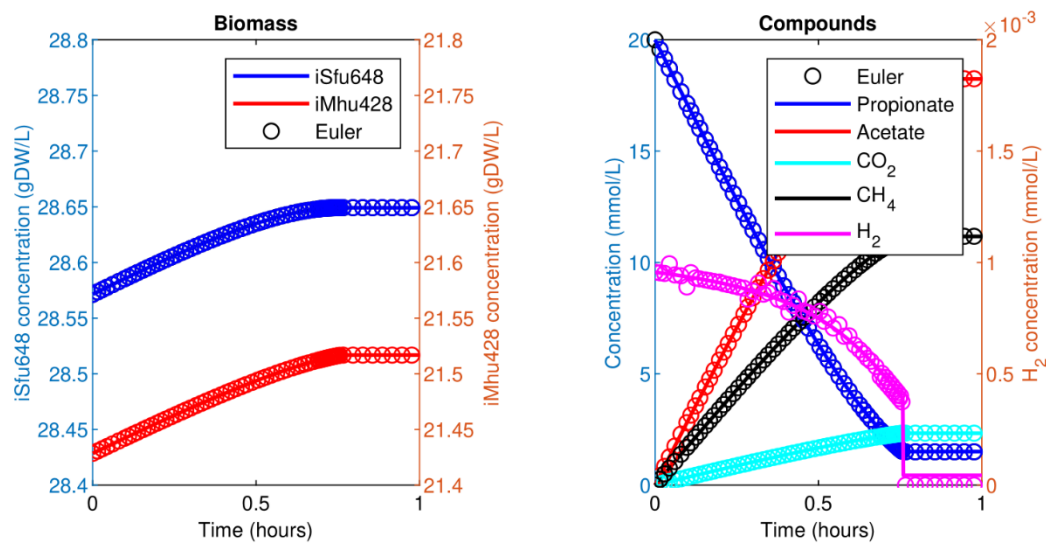
257

258

259 **Table 2. Model parameters and initial biomass concentrations for Example 2.**

Model	$\mu$ (1/d)	$v_{max}^a$ (mmol/gD W/h)	$K_s$ (mM)	NGAM (mmol ATP/gDW/h)	Initial biomass (gDW/L)
<i>S. fumaroxidans</i> iSfu648	0.15 [27]	1.1738	2.7 [28]	0.14 [18]	28.57
<i>M. hungatei</i> iMhu428	1.2 [27]	27.6	0.006 [27]	0.025 [18]	21.43

260 <sup>a</sup>Was chosen such that the maximal FBA-predicted growth rate matched the specific growth rate  $\mu$   
 261 reported in first table column.

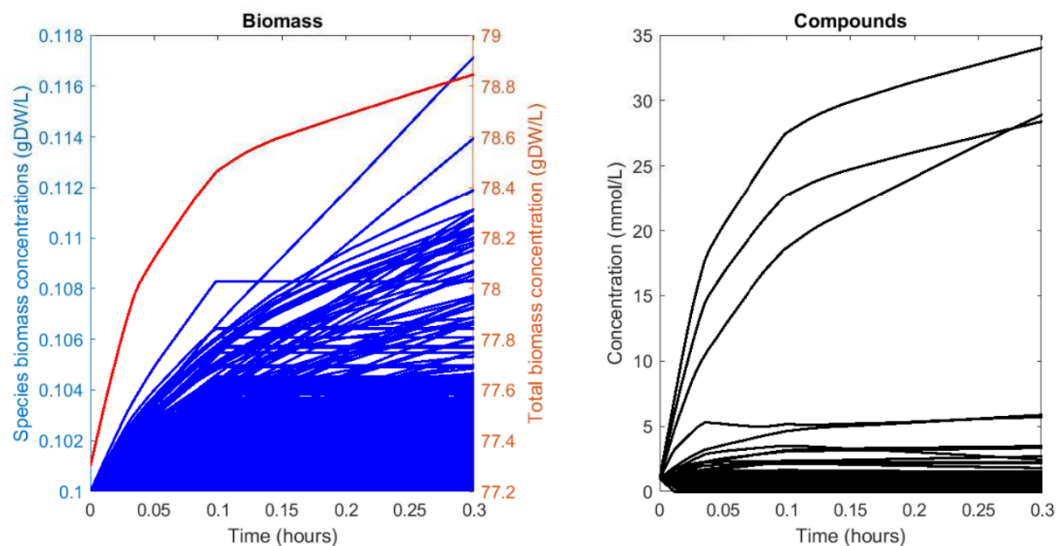


262

263 **Fig 3. Simulating a binary, syntrophic batch culture.** Propionate is utilized by *S. fumaroxidans* and  
 264 converted to acetate, CO<sub>2</sub>, and H<sub>2</sub>. *M. hungatei* then converts CO<sub>2</sub> and H<sub>2</sub> to CH<sub>4</sub>. Both Matlab's  
 265 ode15s ODE solver (lines) and  $\mu$ bialSim's novel augmented forward Euler method (symbols, every  
 266 15th data point is plotted) lead to similar results. As H<sub>2</sub> is faster consumed than produced, the time  
 267 step size gets frequently reduced, most notably just prior to the depletion of propionate after which  
 268 growth of both populations ceases.

## 269 Human gut microbiome

270 To simulate a human gut microbiome, the AGORA model collection (Version 1.01) comprising 773  
271 microbial human gut species was used [29]. Maximal substrate uptake rates ( $v_{max}$ ) were taken from  
272 the individual SBML models, which were configured to mimic a typical western diet [29]. Exchange  
273 reactions in individual models were automatically identified by searching for “EX\_” in reaction  
274 names. Pool compounds were automatically configured by considering only those exchange reaction  
275 which had at least one flux boundary which was neither zero nor unlimited, resulting in 166 pool  
276 metabolites if all 773 models are considered in the simulation. Monod constants for compound  
277 uptake were set to 0.01 mM for all pool compounds. Batch growth was simulated by setting initial  
278 pool compound concentrations to 1.0 mM for all compounds, and initial biomass concentration to  
279 0.1 gDW/L for all microbial species. Simulation results (requiring 7.2 days of simulation time using the  
280 augmented forward Euler method) indicate an initial short period of rapid growth which is followed  
281 by a prolonged period of slow growth (Fig. 4).



282

283 **Fig 4. Simulating a 773 species gut microbiome with 166 pool compounds.** Total biomass growth  
284 slows down as compounds become depleted. Growth for some species ceases early on while others  
285 are able to maintain fast growth rates until the end of the simulation.

## 286 Availability and Future Directions

287  $\mu$ bialSim is licensed under the GNU General Public License v3.0 and available for download at  
288 <https://git.ufz.de/UMBSysBio/microbialsim> (or `git clone`  
289 `https://git.ufz.de/UMBSysBio/microbialSim.git`). The simulator can make use of  
290 Matlab's support for parallel loop execution (`parfor`, option `solverPar.parallel`) for solving  
291 individual FBA problems in one time step. However, the observed speed-up remained far below the  
292 expectation of an almost linear speed-up. This is due to the non-persistence of worker processes  
293 executing individual loop iterations, requiring the repeated copying of FBA model structures to the  
294 workers' memory in each time step. A future version of  $\mu$ bialSim shall feature persistent workers to  
295 better utilize current multicore computing architectures. Besides these technical improvements, non-  
296 metabolic interactions as well as chemical activity among pool compounds and non-constant  
297 chemostat operating conditions can be implemented in future versions of  $\mu$ bialSim. Furthermore,  
298 reactor headspace and corresponding gas exchange processes can be included to ease comparison of  
299 simulation results with experimental data.

## 300 References

- 301 1. Dutta A, Dutta Gupta S, Gupta A, Sarkar J, Roy S, Mukherjee A, et al. Exploration of deep  
302 terrestrial subsurface microbiome in Late Cretaceous Deccan traps and underlying Archean  
303 basement, India. *Sci Rep.* 2018;8: 17459. doi:10.1038/s41598-018-35940-0
- 304 2. Gould AL, Zhang V, Lamberti L, Jones EW, Obadia B, Korasidis N, et al. Microbiome  
305 interactions shape host fitness. *Proc Natl Acad Sci U S A.* 2018;115: E11951–E11960.  
306 doi:10.1073/pnas.1809349115
- 307 3. Deleon-Rodriguez N, Lathem TL, Rodriguez-R LM, Barazesh JM, Anderson BE, Beyersdorf AJ, et  
308 al. Microbiome of the upper troposphere: Species composition and prevalence, effects of



- 309 tropical storms, and atmospheric implications. *Proc Natl Acad Sci U S A*. 2013;110: 2575–2580.  
310 doi:10.1073/pnas.1212089110
- 311 4. Widder S, Allen RJ, Pfeiffer T, Curtis TP, Wiuf C, Sloan WT, et al. Challenges in microbial  
312 ecology: building predictive understanding of community function and dynamics. *ISME J*.  
313 2016;10: 2557–2568. doi:10.1038/ismej.2016.45
- 314 5. Succurro A, Ebenhöf O. Review and perspective on mathematical modeling of microbial  
315 ecosystems. *Biochem Soc Trans*. 2018; doi:10.1042/BST20170265
- 316 6. Song H-S, Cannon WR, Beliaev AS, Konopka A. Mathematical Modeling of Microbial  
317 Community Dynamics: A Methodological Review. *Processes*. 2014;2: 711–752.  
318 doi:10.3390/pr2040711
- 319 7. Bosi E, Bacci G, Mengoni A, Fondi M. Perspectives and Challenges in Microbial Communities  
320 Metabolic Modeling. *Front Genet*. 2017;8: 88. doi:10.3389/fgene.2017.00088
- 321 8. Biggs MB, Medlock GL, Kolling GL, Papin JA. Metabolic network modeling of microbial  
322 communities. *Wiley Interdiscip Rev Syst Biol Med*. 2015;7: 317–334. doi:10.1002/wsbm.1308
- 323 9. Zomorodi AR, Islam MM, Maranas CD. d-OptCom: Dynamic multi-level and multi-objective  
324 metabolic modeling of microbial communities. *ACS Synth Biol*. 2014;3: 247–57.  
325 doi:10.1021/sb4001307
- 326 10. Gomez JA, Höffner K, Barton PI. DFBAlab: a fast and reliable MATLAB code for dynamic flux  
327 balance analysis. *BMC Bioinformatics*. 2014;15: 409. doi:10.1186/s12859-014-0409-8
- 328 11. Chiu H-C, Levy R, Borenstein E. Emergent biosynthetic capacity in simple microbial  
329 communities. *PLoS Comput Biol*. 2014;10: e1003695. doi:10.1371/journal.pcbi.1003695
- 330 12. Louca S, Doebeli M. Calibration and analysis of genome-based models for microbial ecology.  
331 *Elife*. 2015;4: 1–17. doi:10.7554/eLife.08208

- 332 13. Harcombe WR, Riehl WJ, Dukovski I, Granger BR, Betts A, Lang AH, et al. Metabolic resource  
333 allocation in individual microbes determines ecosystem interactions and spatial dynamics. *Cell*  
334 *Rep.* 2014;7: 1104–1115. doi:10.1016/j.celrep.2014.03.070
- 335 14. Karp PD, Latendresse M, Paley SM, Kruppenacker M, Ong QD, Billington R, et al. Pathway  
336 tools version 19.0 update: Software for pathway/genome informatics and systems biology.  
337 *Brief Bioinform.* 2016;17: 877–890. doi:10.1093/bib/bbv079
- 338 15. Bauer E, Zimmermann J, Baldini F, Thiele I, Kaleta C, Noronha A. BacArena: Individual-based  
339 metabolic modeling of heterogeneous microbes in complex communities. *PLOS Comput Biol.*  
340 2017;13: e1005544. doi:10.1371/journal.pcbi.1005544
- 341 16. Varma A, Palsson BO. Stoichiometric flux balance models quantitatively predict growth and  
342 metabolic by-product secretion in wild-type *Escherichia coli* W3110. *Appl Environ Microbiol.*  
343 1994;60: 3724–31.
- 344 17. Koch S, Benndorf D, Fronk K, Reichl U, Klamt S. Predicting compositions of microbial  
345 communities from stoichiometric models with applications for the biogas process. *Biotechnol*  
346 *Biofuels.* 2016;9: 17. doi:10.1186/s13068-016-0429-x
- 347 18. Hamilton JJ, Calixto Contreras M, Reed JL. Thermodynamics and H<sub>2</sub> Transfer in a  
348 Methanogenic, Syntrophic Community. *PLOS Comput Biol.* 2015;11: e1004364.  
349 doi:10.1371/journal.pcbi.1004364
- 350 19. Mahadevan R, Edwards JS, Doyle FJ. Dynamic Flux Balance Analysis of Diauxic Growth in  
351 *Escherichia coli*. *Biophys J.* 2002;83: 1331–1340. doi:10.1016/S0006-3495(02)73903-9
- 352 20. Heirendt L, Arreckx S, Pfau T, Mendoza SN, Richelle A, Heinken A, et al. Creation and analysis  
353 of biochemical constraint-based models: the COBRA Toolbox v3.0. *Nat Protoc.* 2019;14: 639–  
354 702. doi:10.1038/s41596-018-0098-2

- 355 21. von Kamp A, Thiele S, Hädicke O, Klamt S. Use of CellNetAnalyzer in biotechnology and  
356 metabolic engineering. *J Biotechnol.* 2017; doi:10.1016/j.jbiotec.2017.05.001
- 357 22. Lewis NE, Hixson KK, Conrad TM, Lerman JA, Charusanti P, Polpitiya AD, et al. Omic data from  
358 evolved *E. coli* are consistent with computed optimal growth from genome-scale models. *Mol*  
359 *Syst Biol.* 2010;6: 390. doi:10.1038/msb.2010.47
- 360 23. Segrè D, Vitkup D, Church GM. Analysis of optimality in natural and perturbed metabolic  
361 networks. *Proc Natl Acad Sci U S A.* 2002;99: 15112–15117. doi:10.1073/pnas.232349399
- 362 24. Succurro A, Segrè D, Ebenhöf O. Emergent Subpopulation Behavior Uncovered with a  
363 Community Dynamic Metabolic Model of *Escherichia coli* Diauxic Growth. *mSystems.* 2019;4:  
364 e00230-18. doi:10.1128/msystems.00230-18
- 365 25. Richards MA, Lie TJ, Zhang J, Ragsdale SW, Leigh JA, Price ND. Exploring hydrogenotrophic  
366 methanogenesis: A genome scale metabolic reconstruction of *Methanococcus maripaludis*. *J*  
367 *Bacteriol.* 2016;198: 3379–3390. doi:10.1128/JB.00571-16
- 368 26. Weinrich S, Nelles M. Critical comparison of different model structures for the applied  
369 simulation of the anaerobic digestion of agricultural energy crops. *Bioresour Technol.*  
370 2015;178: 306–312. doi:10.1016/j.biortech.2014.10.138
- 371 27. Stams AJM, Plugge CM, de Bok FAM, van Houten BHGW, Lens P, Dijkman H, et al. Metabolic  
372 interactions in methanogenic and sulfate-reducing bioreactors. *Water Sci Technol.* 2005;52:  
373 13–20. doi:10.2166/wst.2005.0493
- 374 28. Batstone DJ, Keller J, Angelidaki I, Kalyuzhnyi S V, Pavlostathis SG, Rozzi A, et al. The IWA  
375 Anaerobic Digestion Model No 1 (ADM1). *Water Sci Technol.* 2002;45: 65–73.
- 376 29. Magnúsdóttir S, Heinken A, Kutt L, Ravcheev DA, Bauer E, Noronha A, et al. Generation of  
377 genome-scale metabolic reconstructions for 773 members of the human gut microbiota. *Nat*

378            Biotechnol. 2017;35: 81–89. doi:10.1038/nbt.3703

379

380

## 381 Supplemental Material

### 382 Installing $\mu$ bialSim

383 The simulator  $\mu$ bialSim is implemented as Matlab code and can be obtained from the UFZ git server  
384 at <https://git.ufz.de/UMBSysBio/microbialsim> or via `git clone`  
385 `https://git.ufz.de/UMBSysBio/microbialSim.git`.  $\mu$ bialSim can be configured to use  
386 the COBRA Toolbox or CellNetAnalyzer for performing FBA calculations. The provided examples make  
387 use of the former. After installing the COBRA Toolbox, the appropriate path needs to be configured in  
388 lines 87ff in the main simulator file `microbialSimMain.m`.

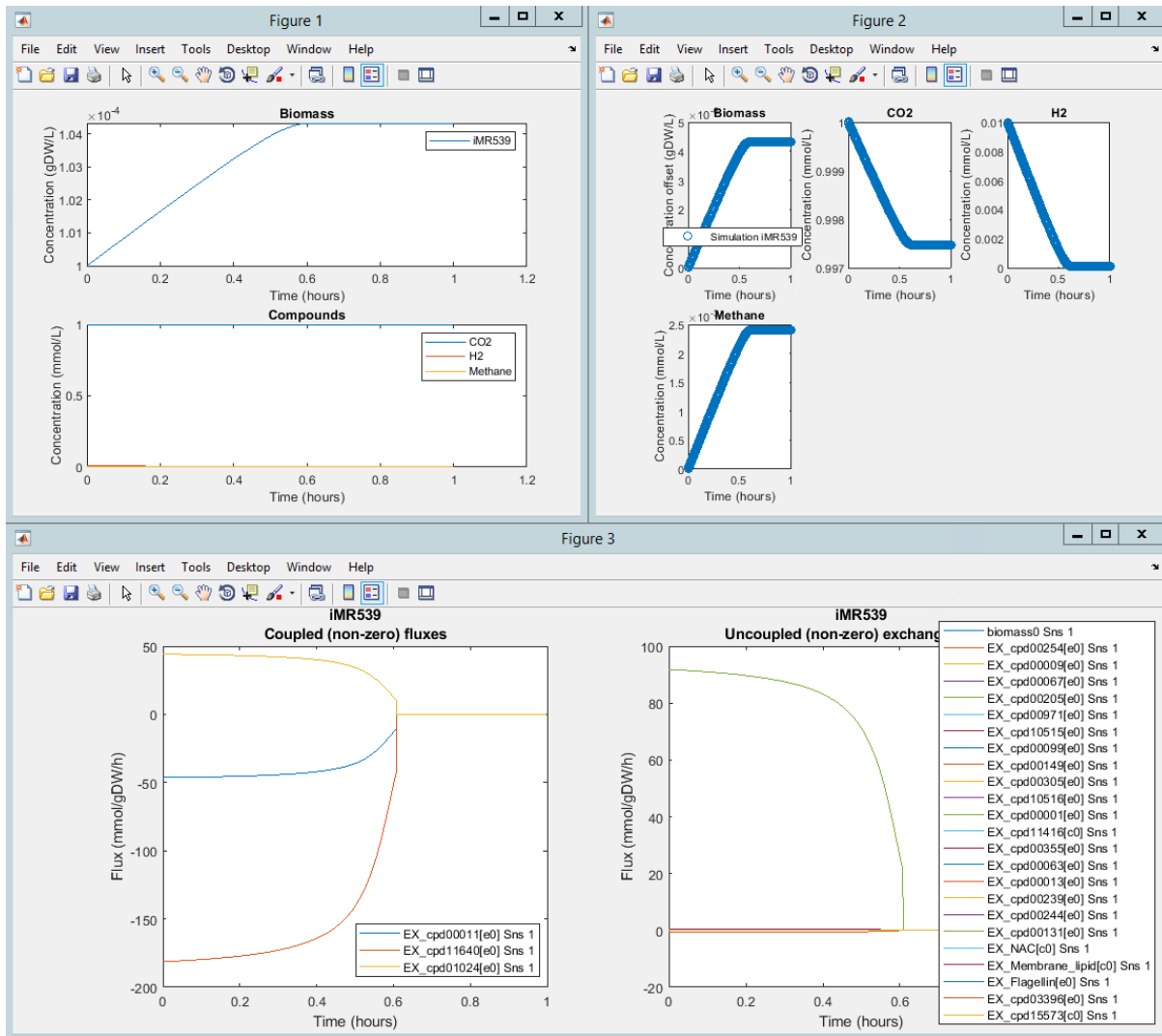
### 389 Simulation output

390 Two files are generated at the end of the simulation with a date and time stamp in the filename  
391 indicating the start of the simulation. Both files hold Matlab data structures. The file  
392 “\*\_restartInit.mat” records the final state of the simulator and can be used as the initial  
393 conditions to continue the simulation in a subsequent run of  $\mu$ bialSim. The other file holds the  
394 simulated trajectory in the Matlab structure `trajectory`. The fields `time`, `compounds`,  
395 `biomass`, and `mu` hold the time, compound concentrations, biomass concentrations, and specific  
396 growth rates for each integration step. The field `FBA` stores data for each FBA model, including the  
397 temporal dynamics of all metabolic fluxes, and the mass balance for all exchange reactions.

### 398 Running the examples

#### 399 Example 1: methanogenic monoculture

400 The first example in which batch-culture growth of a single hydrogenotrophic species  
401 (*Methanococcus maripaludis*) is simulated can be run with the command  
402 `microbialSimMain(1)`. Once the simulation is finished, the trajectory is automatically visualized  
403 in three Matlab figures (Fig S1).  
404

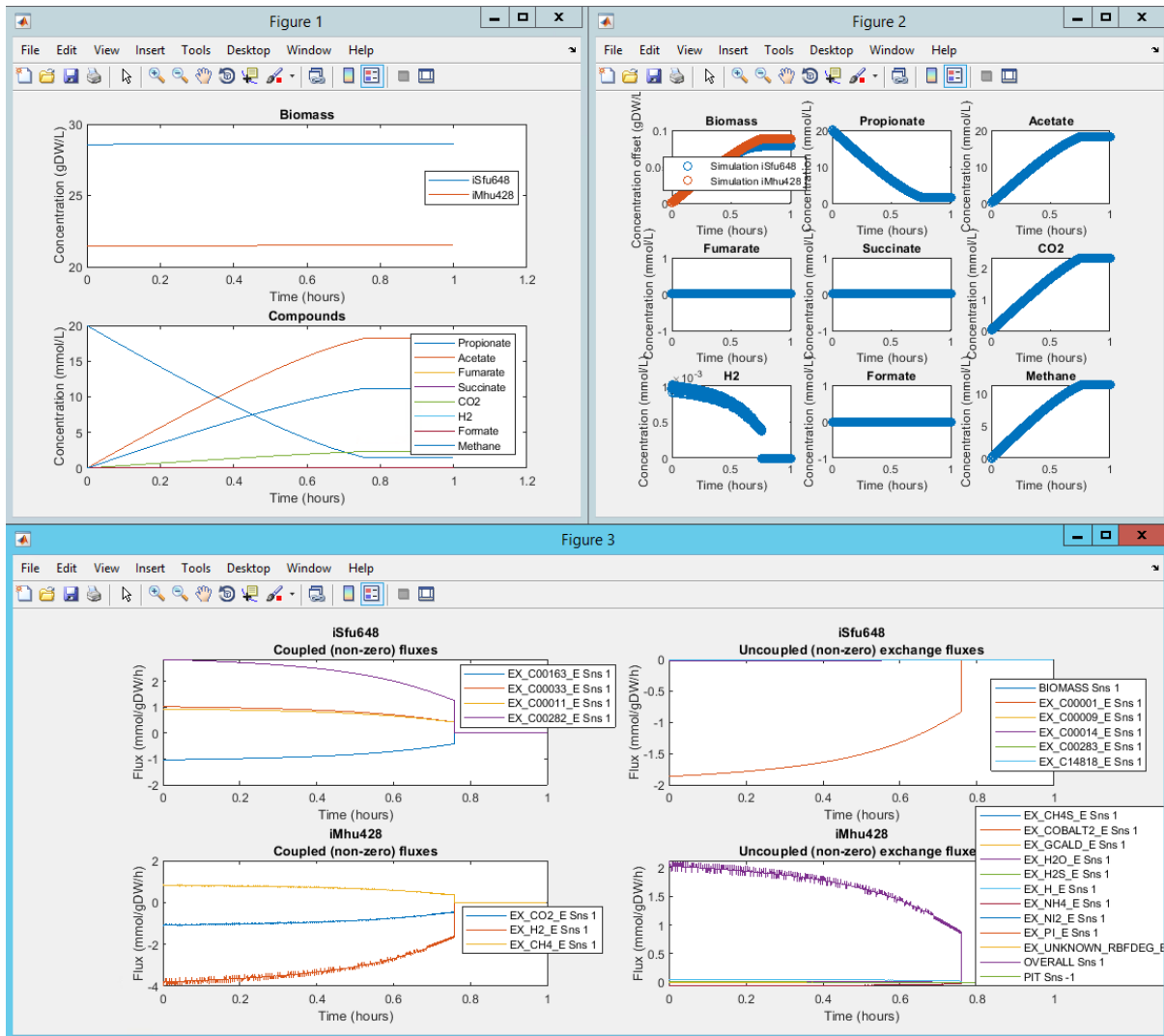


405  
 406 **Fig S1. Automatically generated figure for Example 1.** Simulation trajectory showing all microbiome  
 407 member species and reactor compounds (Figure 1). Plot of biomass concentration as an offset to the  
 408 initial concentration for all microbiome member species and individual plots for all reactor  
 409 compounds (Figure 2). Plotting non-zero exchange fluxes over time which are coupled to reactor  
 410 compounds (left), or not (right) for all microbiome member species (Figure 3).

#### 411 **Example 2: binary syntrophic community**

412 Batch-culture growth of binary methanogenic community is started by  
 413 `microbialSimMain(2)`.

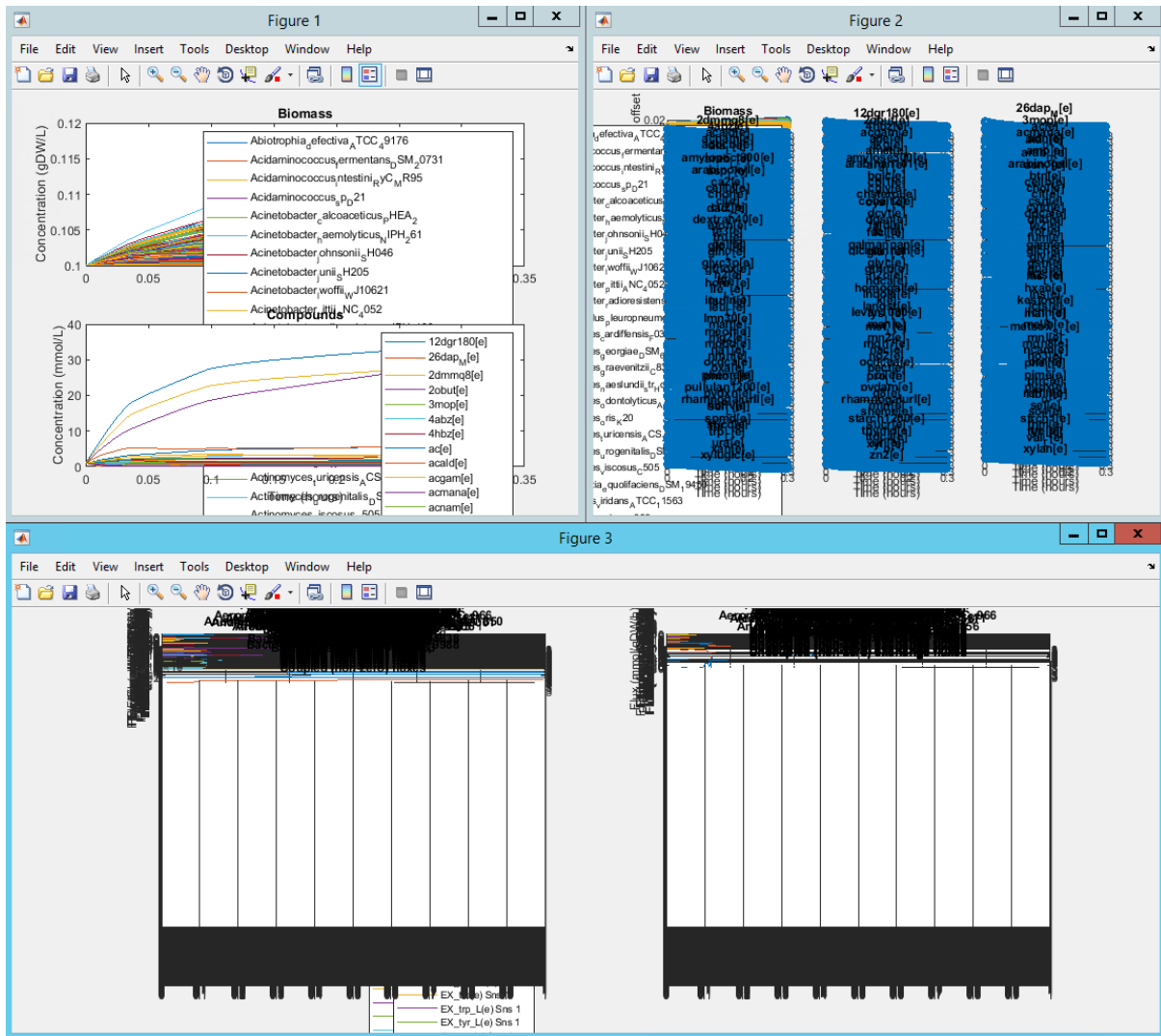
414



415  
 416 **Fig S2. Automatically generated figure for Example 2.** Simulation trajectory showing all microbiome  
 417 member species and reactor compounds (Figure 1). Plot of biomass concentration as an offset to the  
 418 initial concentration for all microbiome member species and individual plots for all reactor  
 419 compounds (Figure 2). Plotting non-zero exchange fluxes over time which are coupled to reactor  
 420 compounds (left), or not (right) for all microbiome member species (Figure 3).  
 421

### 422 Example 3: human gut microbiome with 773 species

423 Running Example 3 first requires the unpacking of the file AGORA-1.01-Western-Diet.zip  
 424 containing the AGORA model collection. Note that for running the simulation with all species, 64GB  
 425 of RAM are necessary (loading models as a Matlab data structure after the initial loading as SBML  
 426 files cuts memory demand in half). The simulation of batch growth can then be started by  
 427 `microbialSimMain(3)`. Simulation time can considerably be reduced by setting the parameter  
 428 `solverPars.maxDeviation` to "inf" in `microbialSimMain.m` at the expense of  
 429 numerical accuracy. Note that also arbitrary subsets of the model collection can be selected for the  
 430 simulation (see commented example in the code).  
 431



432  
 433 **Fig S3. Automatically generated figure for Example 3.** Simulation trajectory showing all microbiome  
 434 member species and reactor compounds (Figure 1). Plot of biomass concentration as an offset to the  
 435 initial concentration for all microbiome member species and individual plots for all reactor  
 436 compounds (Figure 2). Plotting non-zero exchange fluxes over time which are coupled to reactor  
 437 compounds (left), or not (right) for all microbiome member species (Figure 3).